Thermal Equations of State of B2-structured Rubidium Halides RbCl, RbBr and RbI

R. Farla[1*], A. Néri[2], M. Pöppelbaum[3], K. Glazyrin[1]

[1]Deutsches Elektronen-Synchrotron DESY, Notkestr. 85, 22607 Hamburg, Germany

[2]Université de Lille, CNRS, INRAE, Centrale Lille, UMR 8207 - UMET - Unité Matériaux et Transformations, F-59000 Lille, France

[3]Bayerisches Geoinstitut, Universität Bayreuth, 95440 Bayreuth, Germany

*Corresponding author: robert.farla@desy.de

Abstract

In this study, we determined the thermal equations of state (EoS) for rubidium chloride (RbCl), rubidium bromide (RbBr), and rubidium iodide (RbI) in the B2 (CsCl-type) structure. We conducted *in situ* energy-dispersive X-ray diffraction measurements at high pressures (up to 26 GPa) and temperatures (up to 1800 K) using a Large Volume Press (LVP). Pressures were calibrated using CsCl, Mo, and Pt in the same cell assemblies. For each B2-structured Rb halide, the parameter V_0 (unit cell volume at room pressure) was estimated from additional diamond anvil cell (DAC) experiments at 300 K. Using the third-order Birch-Murnaghan equation and the Mie-Grüneisen-Debye thermal model, we derived the thermoelastic parameters for each phase: RbCl: K_0 = 19.89(8) GPa, K_0' = 5.00(2), γ_0 = 1.96(4), q = 1.05(9), RbBr: K_0 = 16.28(4) GPa, K_0' = 5.28(2), γ_0 = 2.18(14), q = 1.52(24), RbI: K_0 = 13.69(4) GPa, K_0' = 4.95(1), γ_0 = 2.21(7), q = 1.42(10). These parameters represent the isothermal bulk modulus (K_0), its pressure derivative (K_0'), the Grüneisen parameter (γ_0) and the logarithmic volume dependence of the Grüneisen parameter (q). The newly derived EoS for rubidium halides provide effective pressure markers above 0.5 GPa, as they remain stable across wide pressure and temperature ranges. Additionally, RbCl and RbBr offer improved X-ray transmission compared to CsCl. These EoS can be combined with a secondary metallic phase to estimate pressure and temperature in the absence of a thermocouple, taking advantage of the large differences in thermal expansion between halides and metals.

Keywords: *High-pressure*, *X-ray diffraction*, *Equation of State*, *Rubidium halides*, *Thermodynamics*

1. Introduction

In the 1970s and 80s, 2nd generation storage rings, with new insertion devices such as wigglers, advanced high-pressure studies away from laboratory X-ray sources tremendously. However, the photon flux at high X-ray energies (> 30 keV) remained limited, requiring X-ray transmissive materials for *in situ* X-ray diffraction (XRD) measurements under high pressure. For this and other reasons, NaCl became an established pressure standard [1–4], but its relatively low-temperature melting curve [5] and B1 (NaCl-type) to B2 (CsCl-type) transition around 24 GPa [6], limit its use for *in situ* studies of the Earth's interior. Although many additional materials, MgO and particularly metals, have become high-pressure standards for XRD [7,8], halides remain appealing due to their high compressibility and well-characterized B1 to B2 transitions. For example, KCl in the B2 structure has recently garnered attention [9–11]. However, as proposed by Decker (1971) [2] and Köhler *et al.*[12], caesium chloride (CsCl) and rubidium halides (RbCl, RbBr, RbI) are promising alternatives due to their extreme compressibility and steep melting curves with increasing pressure [13]. Note, CsCl is already in its B2 structure at ambient pressure, while Rb halides show stable B2 structures at pressures above 0.5 GPa [14,15]. With 3rd and the advent of 4th generation storage rings offering unprecedented high photon flux and brilliance, X-ray absorption in these higher atomic number (Z) materials is no longer a concern, justifying a renewed focus on them.

This study aims to determine the thermal equation of state (EoS) of RbCl-B2, RbBr-B2, and RbI-B2 in the large volume press (LVP) and improve upon the room-temperature diamond anvil cell (DAC) data from Köhler *et al.*[12]. As such, reference pressure standards are essential. In the DAC, ruby fluorescence is commonly used, as well as common EoS standards such as Au and NaCl. In LVP experiments, MgO is widely used. Although its EoS is well-established e.g., by Tange *et al.*[7], it does not provide the same resolution in peak shift from pressure and temperature changes as CsCl and Rb halides do. Due to CsCl's lower homologous temperature at 1800 K (e.g. T/T_{melt} = 0.72 at 10 GPa, 0.55 at 15 GPa) compared to NaCl (T/T_{melt} = 0.85 at 10 GPa, 0.81 at 15 GPa), the former was selected as the primary pressure marker, supported by additional recent XRD data up to 141 GPa at 300 K [16].

Additionally, we include Pt (intimately mixed with CsCl) and Mo (intimately mixed with the Rb halide samples) as independent pressure markers. Mo is particularly useful because its fluorescence peaks are at low enough energies to avoid interference with diffraction patterns, and its diffraction peaks mostly do not overlap with the Rb halide peaks across the wide pressure-temperature range. Furthermore, Mo crystallites also help pinning grain boundaries, reducing grain growth and minimising spotty XRD patterns in the halide samples when heated up to 1800 K.

The new pressure-volume-temperature (*P*-*V*-*T*) data for RbCl-B2, RbBr-B2, and RbI-B2 obtained in the LVP up to 21 GPa and 1800 K and in the DAC up to 26 GPa (at room temperature), along with comprehensive thermal EoS and thermodynamic analysis, aim to promote Rb halides as pressure standards for future high-pressure, high-temperature (HPHT) studies using *in situ* X-ray diffraction in both LVP and DAC setups. These thermal EoS may also be combined with a second metallic phase to estimate pressure and temperature in the absence of a thermocouple [17,18], leveraging the large differences in thermal expansion between halides and metals.

2. Experimental Methods

2.1. X-ray Diffraction Setups

In situ X-ray diffraction (XRD) experiments were conducted at the Deutsches Elektronen-Synchrotron (DESY) facility, using the 6-ram Large Volume Press (LVP) 'Aster-15' at beamline station P61B and a diamond anvil cell (DAC) at the Extreme Conditions Beamline P02.2 [19,20]. The diffraction set ups are explained in these papers (e.g. see Fig. 7 in Farla *et al.* [20] for the LVP station P61B).

At P61B, high-energy white beam X-rays are delivered by an array of 10 damping wigglers, and energy-dispersive X-ray diffraction (ED-XRD) was performed using a germanium (Ge) point detector. This detector was calibrated in the energy range of 30–160 keV using a 4096-channel digital analyzer. The channel-energy relationship was fitted with a quadratic equation based on known X-ray emissions from the ^{57}Co and ^{133}Ba radionuclides. The detector's position was calibrated at a diffraction angle of 4.9964(5)° using the LaB_6 NIST standard [21] and a collimator-slit system. The horizontal opening of the collimator slit was set to 0.03 mm, while the receiving slits were set to 0.5 mm, yielding an approximate gauge volume length of 1.7 mm, as determined by ray-tracing calculations and measurements. Since most samples in the cell assembly had a diameter of ~2 mm, ED-XRD diffraction patterns were therefore largely free from contributions from surrounding materials. Typical XRD acquisition times ranged from 120 to 240 seconds, depending on experimental conditions, with the LVP oscillating between -3° and 5° during acquisitions to improve powder diffraction statistics.

At P02.2, a monochromatic beam with a wavelength of 0.2904 Å (42.69 keV) was focused to 2 × 2 μm^2 (full width at half maximum), and angle-dispersive X-ray diffraction (AD-XRD) was performed employing a Perkin Elmer XRD1621 flat panel detector. The sample-to-detector distance and detector parameters were calibrated using polycrystalline CeO_2. For our ambient temperature studies, we used symmetric DACs with an effective X-ray aperture of ~64° and equipped with Boehler-Almax diamonds [22] with 300 µm culet size. Small polycrystalline flakes of RbI and RbCl were loaded in a single DAC. Another DAC contained a small flake of RbBr. The flakes of irregular form had a dimension of ~30-40 µm in the plane of the diamond culet and did not exceed 10 µm in thickness. In both cases, Re gaskets were pre-indented to 40-45 µm prior to sample loading. He (helium) was used as pressure medium, and within the sample chamber, we also placed small ruby spheres for pressure determination[23].

Samples and Cell Assemblies

The starting materials were purchased as fine-grained powders with high purity: CsCl ≥ 99.9% (Roth Chemicals), Pt ≥ 99.9%, Mo 99.95% (Alfa Aesar), RbCl 99.975%, RbBr 99.8%, and RbI 99.8% (Thermo Fisher Scientific). For the LVP runs, mixtures by weight of CsCl + Pt (1:1.76), RbCl + Mo (1.58:1), RbBr + Mo (1.15:1), and RbI + Mo (1:1.05) were cold-pressed into 0.3–0.4 mm thick discs, 2 mm in diameter. Ethanol was used in an agate mortar to homogeneously mix the halide and metal powders before cold-pressing. The discs were stored in a vacuum oven at 100°C until use, to prevent absorption of humidity. For the DAC experiments, RbCl, RbBr, and RbI powders were used without mixing, with ruby fluorescence acting as the pressure sensor.

Cell assemblies with similar designs but different sizes were employed for the HPHT experiments in the LVP (Fig. S1). The ‘14/7’ assembly, used for experiments up to 10 GPa (BT792, BT793), featured a graphite heater and a Cr-MgO pressure medium with a 14 mm octahedral edge length (OEL) and 7 mm truncated edge length (TEL) anvils in a Kawai geometry. In the ~2 mm sample stack, 50 µm Mo foils separated each sample from each other, including the CsCl + Pt pressure marker. The stack was surrounded by an *h*BN sleeve in the heater's hot zone. A type-C W95%Re5%–W74%Re26% thermocouple, positioned between the CsCl + Pt pressure marker and the sample stack, minimized uncertainty in temperature measurements. The ‘10/5’ assembly, designed for experiments up to 15 GPa, featured a TiB_2 + *h*BN resistive heater, replacing graphite. In the ‘10/4’ assembly, used up to 21 GPa, the thermocouple junction was positioned between the Rb halide samples, with CsCl + Pt filling gaps around the thermocouple (as shown in Fig. S1). This design helped reduce the sample stack length and minimized temperature gradients in this smaller assembly.

Heating was performed with an AC power supply provided by the Bayerisches Geoinstitut (BGI, University of Bayreuth). At each heating step, the temperature was stabilized within 1 K using an Eurotherm power controller. Using simulation software [24], customized for the used cell assemblies, we estimate a maximum 30 K offset between the thermocouple and the most distant sample, as the temperature gradients could not be directly measured. Temperature measurements were not corrected for the pressure effect on the thermocouple electromotive force (emf). A calibration of type-D thermocouples demonstrated an error of -30 K at 16 GPa and 1173 K, and -20 K at 8 GPa [25]. This suggests that XRD acquisitions at the highest temperatures (1800 K) may correspond to lower actual temperatures by as much as -70 K. After the publication of a type-C thermocouple calibration, the equations of state (EoS) in this study may be revised, though this would only be necessary if different thermocouples are used in future studies.

Experimental Runs and Data Processing

Complementary DAC experiments were conducted to obtain room-temperature (300 K) volume data of RbCl-B2, RbBr-B2 and RbI-B2 up to 26 GPa, as cooling of the LVP assembly and anvils would take several hours. Furthermore, the DAC offers better hydrostatic conditions at room temperature.

We carried out four LVP experiments using three different assemblies with ratios of octahedral edge length to anvil truncation edge length (OEL/TEL) of 14/7, 10/5 and 10/4 (Figure S1) to cover a pressure range from 3 to 21 GPa. The temperature-load and temperature-pressure pathways of each experiment are shown in Figure S2. For each experiment, a suitable starting press load was chosen and upon reaching the first target press load, temperature was increased to 800 K, then decreased to 500 K after 30 min to reduce possible stresses in the samples from cold compression. ED-XRD data of the samples and pressure markers are acquired during each heating cycle, followed by cooling to 500 K and further compression to a higher sample pressure, once for BT792 and BT815 and twice for BT793 and BT795. The highest temperature in several experiments was 1800 K.

Full-profile Le Bail refinement was performed on all ED-XRD diffraction data for CsCl + Pt and Rb halides + Mo to obtain their unit cell volumes (and densities) at each temperature and press load, using GSAS-II software [26]. In the refinements, the space group of the three Rb halides and CsCl in the B2 structure, is $Pm\bar{3}m$ (#221), the space group of Mo is $Im\bar{3}m$ (#229) and that of Pt is $Fm\bar{3}m$ (#225). Typically, in the energy range of 35–160 keV with a Ge detector at 2θ ≈ 5°, around 8 CsCl peaks were included in the refinement, up to 9 peaks for RbCl-B2, 5-6 peaks for RbBr-B2, and 6-7 peaks for RbI-B2. The *hkl* lines included for the halides, varied significantly with experimental conditions depending on pressure, temperature, and peak overlap with Pt and Mo diffraction peaks, and/or fluorescence of Pt and Pb (from detector shielding). For Pt, 4-5 peaks (111, 200, 220, 311, 222) and for Mo, 5 peaks (110, 200, 211, 220, 310) were routinely fitted within the available energy range. During cold compression to the first target press load, broadening of the halide peaks was observed, indicating the presence of differential stresses. The full width at half maximum (FWHM) of these peaks increased from ~0.5 keV to ~1 keV but was fully recovered at the start of data collection at 500 K following annealing at 800 K. In principle, all diffraction peaks maintained a FWHM resolution close to the specifications of the Ge detector (0.4 keV at 60 keV, 0.48 keV at 122 keV). Based on these observations, differential stresses were likely fully relaxed during data collection at all temperatures (500–1800 K).

From the obtained unit cell volumes at known temperatures, pressures were calculated for CsCl, Pt and Mo using the free software EosCross by Farla[18] supported by the BurnMan thermodynamic and geophysics toolkit [27]. In particular, version 1.3 of EosCross (https://gitlab.desy.de/robert.farla/eoscross) offers the option to calculate pressures from several published EoS of these materials simultaneously. The used EoS are the following: CsCl [2,16], Pt [28–30], Mo [8,31,32]. The same software was used to calculate pressures (and pressure differences to CsCl and Mo) with the EoS proposed for RbCl-B2, RbBr-B2 and RbI-B2 in this study. EosCross uses a *P-V-T* correlation matrix to calculate uncertainties in the pressure for each phase, and does not consider the uncertainties in the parameters of the published equations of state. The estimated standard deviations (esd) in the unit cell volume of the phases are reported by GSAS-II after refinement, and we include a 30 K uncertainty in the temperature as mentioned earlier.

2.2. Post-experiment microstructural analysis

The cell assemblies with the samples inside were recovered from all experiments except from the last run (BT815). The octahedra were carefully sectioned in half and impregnated in epoxy resin. Polishing each surface for scanning electron microscopy (SEM) imaging was challenging since no H_2O could be used that would dissolve the halide samples. The samples were carbon-coated and imaged with secondary electrons using the Zeiss Gemini 1530 SEM at BGI. The polishing appears successful, although some gaps and surface roughness could not be avoided. In addition, energy-dispersive X-ray microscopy (EDS) was used to produce various maps of the samples for the absorption edges of Rb, Cl, Br, I, Pt, and Mo (Figs. S4 – S6).

3. Equations of state

Many different approaches exist in the literature to calculate the thermoelastic parameters of materials and how its volume and density varies with pressure and/or temperature. The free software EoSFit7 [33,34] offers many choices to reliably obtain values of the EoS parameters with estimated standard deviations in the parameters. We fitted the *P-V-T* data of the Rb halides using this software and report the results in Tables 1 and 2.

3.1. Isothermal equation of state

Conventional methods for calculation of the isothermal (300 K) compression of solids are the 3rd order Birch-Murnaghan (BM3) [35] and Vinet [36] EoS. Typically, below 100 GPa, the Vinet and BM3 EoS may give practically identical results [31], and which one to use is a matter of preference. In this study, the maximum pressure is not extremely high, hence the BM3 EoS is considered here:

$$P(V)=\frac{3}{2}K_0\left[\left(\frac{V_0}{V}\right)^{7/3}-\left(\frac{V_0}{V}\right)^{5/3}\right]\left\{1+\frac{3}{4}\left(K_0^{'}-4\right)\left[\left(\frac{V_0}{V}\right)^{2/3}-1\right]\right\}, \quad (1)$$

where V is the high-pressure unit cell volume, V_0 is the unit cell volume at reference pressure, K_0 is the isothermal bulk modulus and K_0' its pressure derivative. Note that the parameters for a particular EoS produce values that cannot be interchangeably used with other EoS to calculate pressures.

3.2. Thermal pressure

Two common approaches are used to calculate the effect of temperature on volume expansion. First, the BM3 EoS is recalculated at successively higher temperatures along the isotherms, here referred to as HT-BM3. Note that this approach does not meet the thermodynamic requirement $(\partial K_T/\partial T)_P=0$ at 0 K. Notwithstanding, the temperature effect on the bulk modulus (K_T; replacing K_0 in Eq. 1) is given by:

$$K_T=K_{T0}+(\partial K_T/\partial T)_P(T-T_0), \quad (2)$$

where $(\partial K_T/\partial T)_P$ is the temperature derivative of the bulk modulus and T_0 is the reference temperature (300 K). We assume $K_T^{'}$ to be constant with temperature, but it can adopt a similar expression as K_T.

The temperature effect on the unit cell volume at reference pressure (V_{0T}) (replacing V_0 in Eq. 1) is given by:

$$V_{0T}=V_0\exp\left[\int_{T_0}^{T}\alpha dT\right], \tag{3}$$

$$V_{0T}=V_0*\exp\left[\left(a_0T+a_1T^2/2-a_2/T\right)-\left(a_0T_0+a_1T_0^2/2-a_2/T_0\right)\right], \tag{4}$$

where the thermal expansion coefficient is expressed as:

$$\alpha(T)=a_0+a_1T+a_2T^{-2}, \tag{5}$$

where $\alpha=(1/V)(\partial V/\partial T)_P$ is the volume thermal expansion coefficient [37]. We optimized the parameters $K_{T0}, K_T^{'}, (\partial K_T/\partial T)_P, a_0, a_1$, with V_0 fixed (values obtained from extrapolation of room-temperature DAC data using the BM3 model) to obtain the HT-BM3 EoS for RbCl-B2, RbBr-B2 and RbI-B2. Including a_2 as a variable, does not offer any appreciable improvement to the fitting, hence it was set to zero ($a_2=0$).

Second, a thermal pressure model such as the Mie-Grüneisen-Debye (MGD) thermodynamic approach [38–40] can be used, which explicitly incorporates an approximate model for the vibrational energy. We prefer this approach, because it describes more reliably the temperature dependence of the thermal expansion, and allows internally consistent conversion between isothermal and adiabatic experimental conditions. The formalism can be summarized as follows:

$$\Delta P_{th}=\gamma\left[E_{th}(V,T)-E_{th}(V,T_0)\right]/V, \tag{6}$$

where γ is the Grüneisen parameter, E_{th} is the thermal energy, which is calculated from the Debye model:

$$E_{th}=\frac{9nRT}{(\theta/T)^3}\int_0^{\theta/T}\frac{\xi^3}{e^{\xi}-1}d\xi, \tag{7}$$

where *n* is the number of atoms per formula unit (i.e. 2 for RbCl, RbBr, RbI), R is the ideal gas constant, and θ the Debye temperature. The volume dependence of θ and γ are given by:

$$\theta=\theta_0\exp\left[\left(\gamma_0-\gamma\right)/q\right] \tag{8}$$

$$\gamma=\gamma_0\left(V/V_0\right)^q \tag{9}$$

Note, when $q=0$, γ is constant and equal to γ_0. The values for γ_0 and *q* control the value of the Debye temperature θ, which is advantageous because the *V-T* data can constrain the values of these parameters. Other thermodynamic properties can be calculated from the MGD model, such as the isochoric and isobaric heat capacities C_P and C_V. The MGD thermal pressure ΔP_{th} is thus calculated in addition to the static pressure at 300 K from the BM3 EoS (Eq. 1): $P(V,T)=P(V)+\Delta P_{th}$. For this approach, we fitted K_{T0}, K_T', γ_0 and *q* to the LVP+DAC data, while keeping V_0 and θ_0 fixed. The Debye temperatures were calculated from the elastic constants of the Rb halides [41] using the method outlined by Anderson[42], see Supplementary Materials.

4. Results and interpretations

4.1. Microstructures

Samples recovered from the LVP experiments (Fig. S4 – S6) show good preservation and minimal deformation of the sample stacks, including the CsCl-Pt pressure marker and the thermocouple junction. The Rb halide and Mo grains (initially 3-7 µm) appear to be homogeneously mixed and grain growth does not seem to be significant, suggesting that grain boundary pinning was effective. Note that upon pressure release, the Rb halides would have converted back to the B1 (NaCl-type) structure, which may affect their final microstructure. The EDS maps for the absorption edges of Rb, Cl, Br, I, Pt, and Mo do not show any obvious contamination and the different samples and components can be clearly identified. No obvious chemical reactions, such as changes in composition of Mo mixed with the samples in the Mo discs separating the samples, can be identified.

4.2. DAC experiments

The unit cell volume V_0 of the B2 phases of RbCl, RbBr and RbI at ambient pressure and 300 K cannot be directly obtained, as they are not stable under ambient conditions. Hence, two DAC experiments were carried out (RbCl + RbI and RbBr) at beamline P02.2 up to 26 GPa, using ruby fluorescence as a pressure sensor. Integration of 2D diffraction images into 1D profiles was done using DIOPTAS [43]. Representative diffraction patterns are shown in Figure S7. The lattice parameters as a function of pressure were subsequently extracted by means of JANA2006 [44]. Finally, Le Bail analysis was performed on the diffraction patterns and the resulting high-pressure volumes were fitted by the isothermal BM3 EoS to obtain V_0, K_0 and K' for all three B2 phases of the Rb halides, as shown in Figure 1 and Table S1. These curves are in good agreement with previous data obtained in the DAC [12], although their scattered data produced slightly larger V_0, smaller K_0 and larger K_0' than in this study. In subsequent analysis, the DAC data are combined with LVP data to obtain the complete thermal EoS of Rb halides.

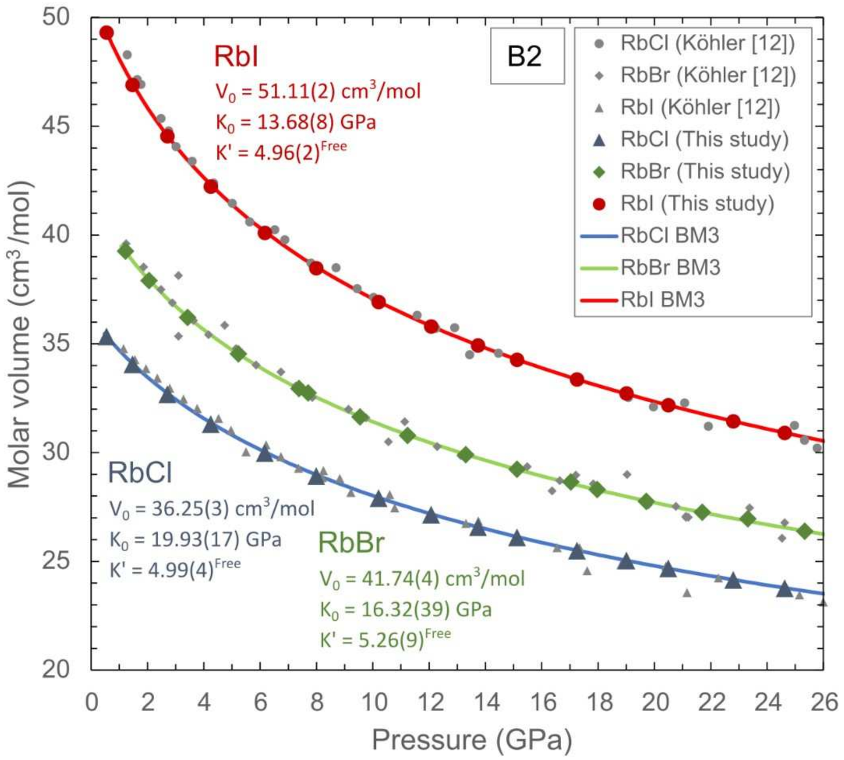

Figure 1. P-V-T data for RbCl, RbBr and RbI in the B2 structure obtained in the DAC, fitted by the 3^{rd} order Birch-Murnaghan (BM3) equation of state indicated by the coloured symbols and curves, respectively. Previous DAC data are shown by the grey symbols [12]. Note, if K' for RbBr is fixed at an intermediate value of 4.98, then V_0 = 41.55(4) cm^3/mol, and K_0 = 17.55(11) GPa.

4.3. LVP experiments

We conducted four in situ ED-XRD experiments using the 'Aster-15' LVP at P61B, following the previously described P-T pathways (Fig. S2). Diffraction patterns were processed via Le Bail full-profile fitting in GSAS-II, and the unit cell volumes of the Rb halides, along with the unit cell volumes and calculated pressures for CsCl, Pt, and Mo, are presented in Tables S2 – S4. The GSAS-II project files for each experiment, including diffraction patterns and corresponding Le Bail refinements, are provided in the Supplementary Materials. Figure 2 shows an example of diffraction patterns at HPHT conditions, refined using the Le Bail method. The background and intensity extraction using this technique provided excellent peak fitting for all phases. Some energy ranges were excluded due to the presence of fluorescence peaks (from Pt and Pb) and occasional diffraction lines from the MgO sleeve.

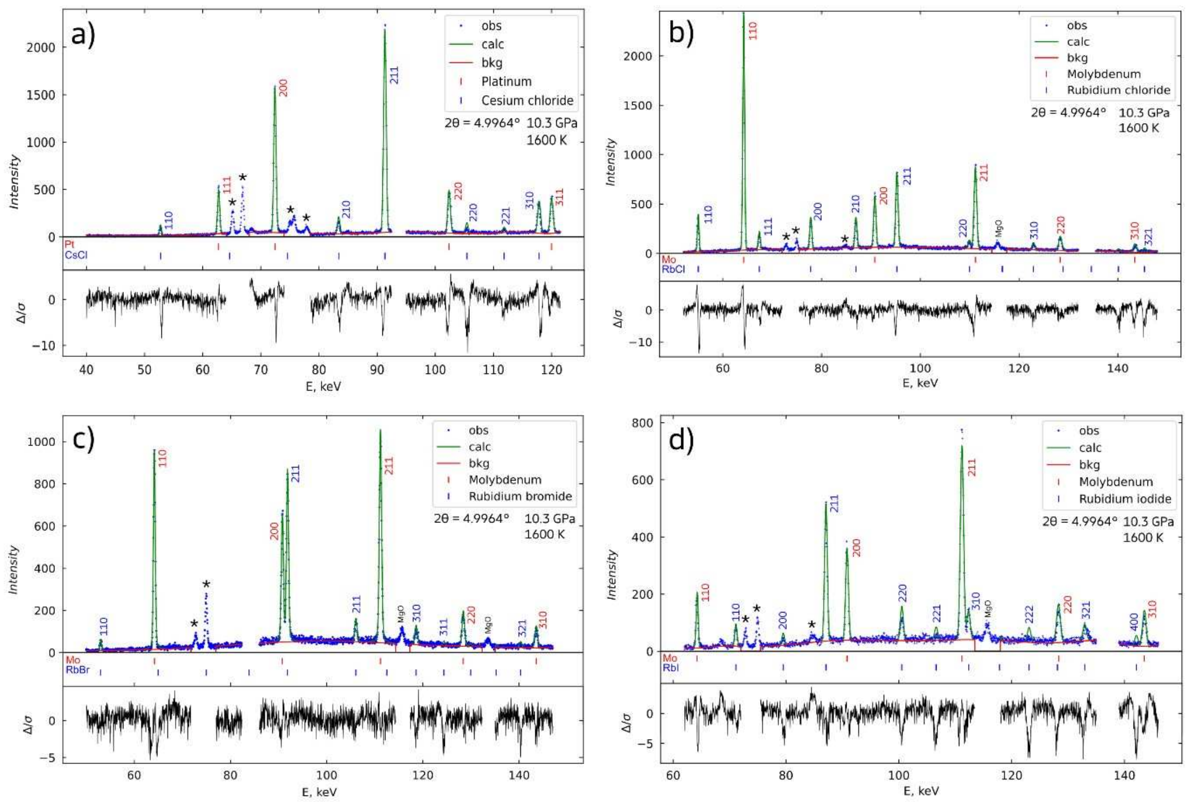

Figure 2. Representative X-ray diffraction patterns of CsCl (panel a), RbCl (panel b), RbBr (panel c) and RbI (panel d) in the B2 structure acquired at 1600 K and 10.3 GPa (BT793). Pt is mixed with CsCl, whereas Mo is mixed with the Rb halides, as shown. The green line in each pattern represents the calculated result after Le Bail refinement in GSAS-II, indicating excellent agreement for all cases. Each refinement includes a polynomial background (12th order, red line). The asterisks indicate the positions of the fluorescence lines for Pb (and Pt in panel a).

We used EoSFit7 [33] to fit the combined *P-V-T* data with the models outlined in the previous section, focusing primarily on the BM3-MGD model. Results for this EoS are shown in Table I, with experimental and model data plotted in Figures 3, 4, and 5 for RbCl-B2, RbBr-B2 and RbI-B2, respectively. Since we measured multiple pressure markers, there was a need to determine which pressures to use for fitting with the BM3-MGD model. We present EoS parameters (Table I) for three cases: (1) using CsCl pressures, (2) using "Mo-weighted" pressures—an average of CsCl and Mo pressures from the RbCl, RbBr, and RbI samples, and (3) fixing the parameters V_0, K_{T0}, and K_T' obtained from the 300 K DAC experiments and only refining the thermal parameters γ_0 and q. In all cases, V_0 was fixed to values obtained from room-temperature DAC data, and the Debye temperatures (θ_0) were calculated for RbCl-B2, RbBr-B2, and RbI-B2 (Supplementary Materials) and fixed in the refinements to avoid unrealistically high values.

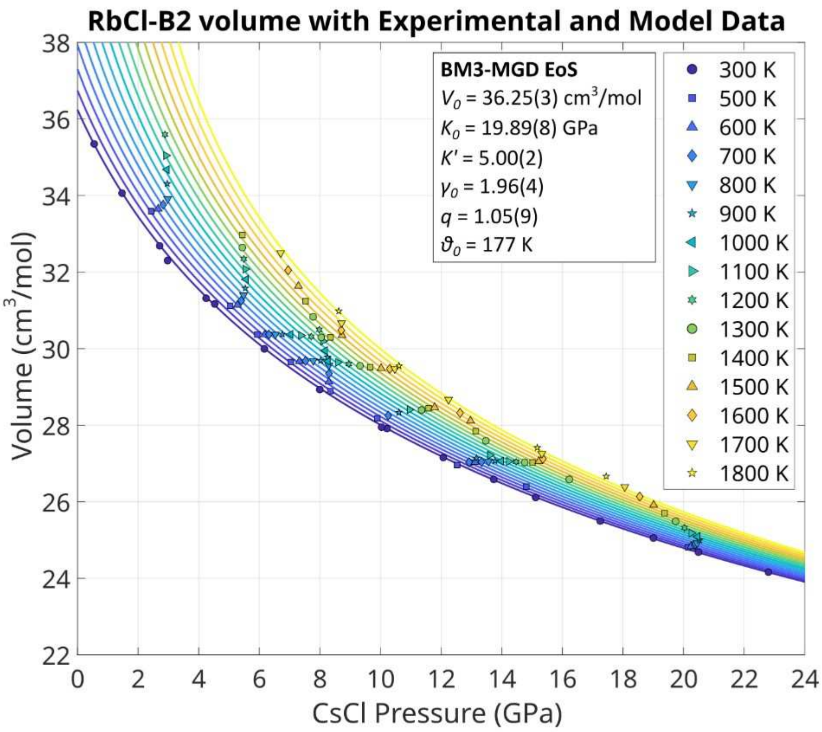

Figure 3. Experimentally obtained unit cell volume and BM3-MGD model data of RbCl-B2 covering a range of pressures and temperatures. The 300 K data are obtained in the DAC and all high-temperature data are obtained in the LVP. The symbols correspond to each temperature step and are colour-coded according to the BM3-MGD isothermal compression curves calculated at the same temperatures. Note, a curve is included for 400 K, but no data were collected at this temperature.

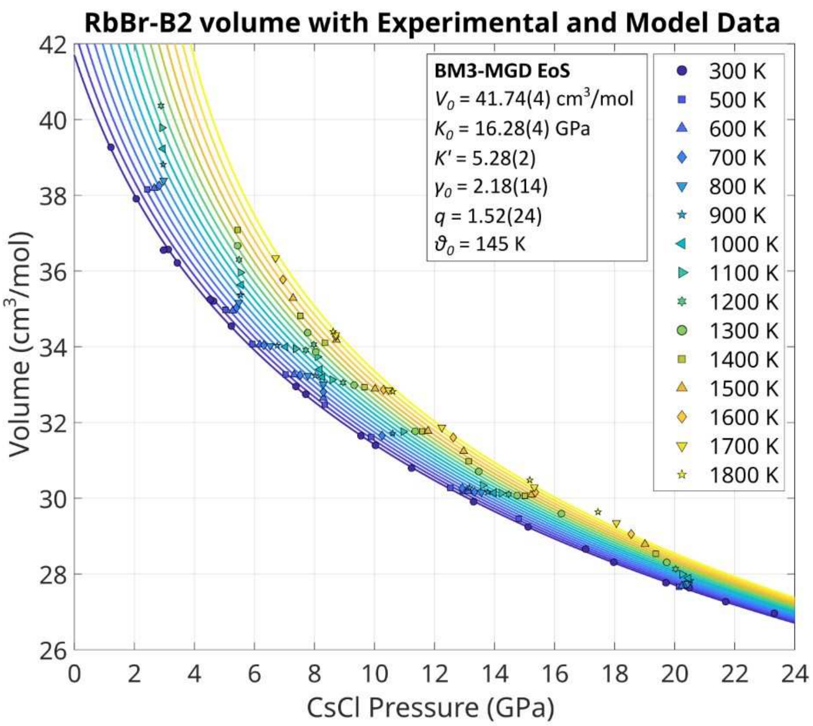

Figure 4. Experimentally obtained unit cell volume and BM3-MGD model data of RbBr-B2 covering a range of pressures and temperatures. The 300 K data are obtained in the DAC and all high-temperature data are obtained in the LVP. The symbols correspond to each temperature step and are colour-coded according to the BM3-MGD isothermal compression curves calculated at the same temperatures. Note, a curve is included for 400 K, but no data were collected at this temperature.

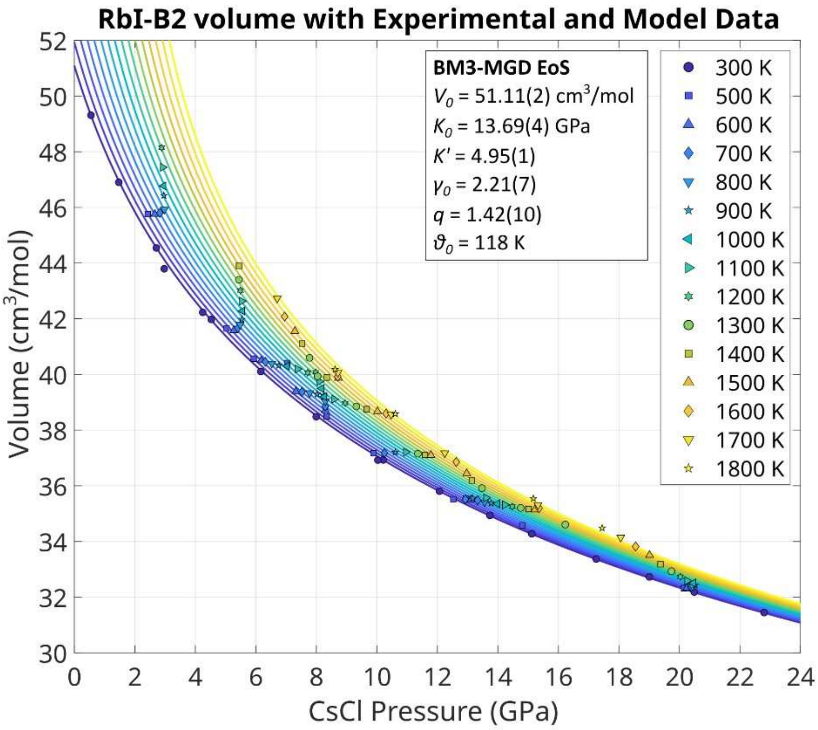

Figure 5. Experimentally obtained unit cell volume and BM3-MGD model data of RbI-B2 covering a range of pressures and temperatures. The 300 K data are obtained in the DAC and all high-temperature data are obtained in the LVP. The symbols correspond to each temperature step and are colour-coded according to the BM3-MGD isothermal compression curves calculated at the same temperatures. Note, a curve is included for 400 K, but no data were collected at this temperature.

The parameters $K_{T0,}$ and $K_T{}'$ show strong agreement across all cases, particularly between cases 1 and 3, and the DAC data align well with previous data by Köhler *et al.* [12] (Fig. 1). However, larger differences emerge between cases 1 and 2 in the thermal parameters of the MGD EoS. The Grüneisen parameter (γ_0) is higher by 0.06 to 0.17 for the Rb halides from case 1 to 2, although still within uncertainties. More notably, the q parameter, describing the Grüneisen power-law in V/V_0, exhibits unusually large values in case 2, up to 2.42 for RbI-B2. An unexpected effect appears to influence pressure calculations at high temperatures (>1100 K) using the Mo and Pt EoS for these metals mixed with the halide samples. This is discussed in Section 5.

Table I. Thermoelastic parameters for RbCl, RbBr, and RbI in the B2 structure obtained using the BM3-MGD EOS. The parameters are obtained using EoSFit7 including weighted errors in the *P-V-T* DAC + LVP data.

	RbCl-B2			RbBr-B2			RbI-B2		
Parameter	(1)	(2)	(3)	(1)	(2)	(3)	(1)	(2)	(3)
V_{0T} (cm³/mol) [a]	36.25(3)	36.25(3)	36.25(3)	41.74(4)	41.74(4)	41.74(4) | 41.55(4)	51.11(2)	51.11(2)	51.11(2)
V_{0T} (Å³) [a]	60.20(2)	60.20(2)	60.20(2)	69.31(7)	69.31(7)	69.31(7) | 68.99(7)	84.87(2)	84.87(2)	84.87(2)
K_{T0} (GPa)	19.89(8)	19.16(23)	19.93[c]	16.28(4)	16.28(5)	16.32[c] | 17.55[c]	13.69(4)	13.61(8)	13.68[c]
K'_T	5.00(2)	5.22(7)	4.99[c]	5.28(2)	5.28(2)	5.26[c] | 4.98[c]	4.95(1)	4.98(3)	4.96[c]

γ_0	1.96(4)	2.03(6)	1.96(4)	2.18(14)	2.25(14)	2.17(13) | 2.11(18)	2.21(7)	2.38(14)	2.22(7)
q	1.05(9)	1.75(13)	1.04(9)	1.52(24)	2.41(23)	1.49(23) | 1.50(32)	1.42(10)	2.42(20)	1.43(10)
θ_0 (K) [b]	177	177	177	145	145	145	118	118	118

a) All V_0 are fixed according to the values obtained from the room temperature DAC data.

b) Debye temperatures are fixed according to calculations (see Supplementary Materials).

c) Fixed parameter.

(1) Parameters calculated using CsCl pressures; (2) and based on Mo-weighted pressures;
(3) refinement of the thermal EoS with K_{T0} and K_0' parameters from DAC data fixed, only free thermal parameters γ_0 and q. For RbBr, K' can be 5.26 (Fig. 1) or a fixed value 4.98, between RbCl (3) and RbI (3). Both cases are considered for evaluating the thermal parameters.

Overall, the *P*-*V*-*T* data (Figures 3-5) closely match the BM3-MGD model (case 1) for RbCl-B2, RbBr-B2, and RbI-B2. This can be seen more clearly by calculating pressures from Rb halide volumes using the BM3-MGD models and comparing these with pressures from CsCl (Figure 6). No clear trends are observed in ΔP (P_{CsCl} - $P_{RbCl,Br,I}$) across the four temperature ranges with increasing reference pressure (P_{CsCl}). Pressure differences remain small (±0.1 GPa) below 6 GPa, increasing to ±0.3 GPa at higher pressures, with most data falling within this range as indicated by the dotted lines (Fig. 6). Interestingly, most outliers in ΔP > ±0.3 GPa lie in the 700-1000 K and 1500-1800 K ranges. The relative volumes (*V*/V_0) of RbCl-B2, RbBr-B2 and RbI-B2 as function of pressure and temperature using the BM3-MGD EoS (case 1 model in Table I) are listed in Tables S5 – S7. These calculated values can be used to benchmark the correct implementation of the EoS published in this study, such as in EosCross [18].

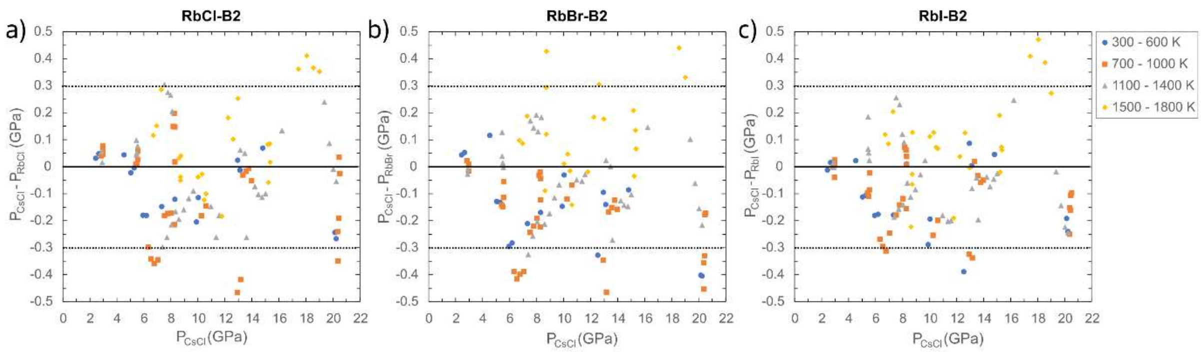

Figure 6. Differences between pressures calculated using EoS of CsCl and those calculated using the BM3-MGD EoS of B2 RbCl (panel a), RbBr (panel b) and RbI (panel c) in this study (case 1, Table I). The data are separated by colour into 4 temperature groups. Most data are plotted between the dotted lines, which are arbitrarily placed at ± 0.3 GPa to guide the eye.

Finally, we used the HT-BM3 EoS, which incorporates thermal expansion calculations [37] with a linear $(\partial K_T/\partial T)_P$ cross-term in EoSFit7. The refined parameters – $K_{T0}, K_T', (\partial K_T/\partial T)_P, a_0, a_1$ – are presented in Table II, with slight differences in K_{T0} and K_T' compared to the BM3-MGD formulation (Table I). As observed also using this EoS, the compressibility of the B2-Rb halides shows a substantial volume reduction, with RbI-B2 experiencing the greatest reduction due to iodine's large atomic radius in the crystal structure. As expected, thermal expansion is highest for RbCl-B2, followed by RbBr-B2, and lowest for RbI-B2, though the effect of temperature on volume diminishes significantly with increasing pressure. Notably, the thermal pressure $(\partial K_T/\partial T)_P$ for halides remains much smaller than that of metals (e.g., -0.0243 GPa/K for Mo [31] vs. -0.0055 GPa/K for RbI in Table II).

Table II. Thermoelastic parameters for RbCl, RbBr, and RbI in the B2 structure obtained using the HT-BM3 EOS. The parameters are obtained using EoSFit7 including weighted errors in the P,V,T of the data.

Parameter	RbCl-B2	RbBr-B2	RbI-B2
V_{0T} (cm^3/mol) [a]	36.25(3)	41.74(4)	51.11(2)
V_{0T} ($Å^3$) [a]	60.20(2)	69.31(7)	84.87(2)
K_{T0} (GPa)	20.11(11)	16.30(5)	13.77(5)
K'_T	4.94(3)	5.27(2)	4.93(2)
$(\partial K_T/\partial T)_P$ (GPa/K)	-0.0079(2)	-0.0069(3)	-0.0053(2)
a_0 (/K)	$6.32(28) \times 10^{-5}$	$5.23(62) \times 10^{-5}$	$6.46(30) \times 10^{-5}$
a_1 (/K^2)	$8.54(68) \times 10^{-8}$	$10.82(149) \times 10^{-8}$	$8.24(81) \times 10^{-8}$

a) All V_0 are fixed according to the values obtained from the room-T DAC data.

Parameters are calculated using CsCl pressures.

5. Discussion

5.1. Chosen strategy and cell assembly behavior at HPHT in the LVP

We opted not to perform decompression-heating cycles as done elsewhere for LVP experiments [e.g. 31], but rather the opposite. This decision was made because grain growth in halides is significant at high temperatures, as observed by Farla[18] and a single heating cycle to 1800 K may result in the permanent disappearance of many diffraction peaks in the Ge point detector. To manage this, we employed compression-heating (*P*-*T*) pathways where each heating cycle was followed by further compression (Fig. S2) in an attempt to crush the grains anew. We believe this approach worked, because good diffraction patterns were preserved throughout the compression-heating cycles, e.g. demonstrated by the many sample peaks in the diffraction patterns at 1600 K towards the end of the experiment BT793 (Fig. 2).

There are some challenges to this approach. The first challenge is that additional care is required to minimise any new stresses in subsequent XRD acquisitions after further compression, which is why we cooled to 500 K (kept constant during further compression), not to room temperature (Fig. S2), and we made sure there were no erratic deviations in the peak positions or significant broadening of the peaks. The other challenge of this method is that first heating results in a significant loss of pressure (especially during subsequent cooling), requiring a substantially higher press load to reach the next pressure target (Fig. S2). This is expected since the most significant gasket flow occurs in the first heating at high temperatures (see BT793, BT795).

The load-pressure-temperature pathways in the experiments are crucial to understanding the trends of data symbols in Figures 3 – 5 (and S8 – S10 in the supplemental). As stated above, it is common in multi anvil LVP experiments that during the first heating at constant load, sample pressure is reduced in the cell assembly (sometimes also during a second heating). A pressure reduction results in a larger unit cell volume, further enhanced by thermal expansion towards higher temperatures. This behaviour results in the 'vertical' to left-leaning trends of data symbols in Figures 3 – 5. Usually, subsequent heating cycles will produce a different behaviour in the high pressure multi anvil cell, no matter whether the press load was increased or not. What happens then is that the thermal expansion of the cell (and sample) dominates and the pressure increase is largely thermal pressure. This results in the quasi 'horizontal' trends of data symbols in Figures 3 – 5. Interestingly, this implies that the unit cell volume of the samples remains constant with increasing temperature and pressure in the LVP, as the effects of both appear to cancel each other out.

For example, consider the case for BT975 (Fig. S2). Upon reaching the target load of 6 MN, the initial CsCl pressure of 12.5 GPa at 500 K was obtained. After the first heating and cooling cycle, the pressure dropped to 10 GPa. Keeping the press load constant at 6 MN, reheating to 1500K caused the pressure to reincrease to ~12 GPa, and subsequent cooling returned the pressure back to ~10.5 GPa at 500 K. This is essentially the effect of thermal pressure from thermal expansion of the whole cell assembly (and sample). To achieve higher pressures, further compression is possible as long as there is sufficient load capacity in the LVP (15 MN) and the anvil gap is not reduced too much (> 100 µm). Subsequent heating at 10.9 MN increased the pressure from ~13 GPa to ~15 GPa at ~1800 K, mainly by the effect of thermal expansion.

5.2. Pressure Deviations at High Temperatures

Pressures calculated for Mo and Pt deviate between each other and significantly from CsCl pressures at high temperatures, despite an expectation that disagreements would occur at lower temperatures where differential stresses are expected to be greater. Generally, calculated Mo pressures are similar to CsCl pressures for most heating runs in the experiments up to about 1100 K, except for heating run 2 of BT793 where they are higher (Fig. S3). What occurs around 1100 K and higher temperatures is unclear, but the calculated Mo pressures are increasingly lower than pressures calculated for CsCl – a difference up to about 1 GPa at 1700-1800 K in many cases. The same effect is seen for Pt, whose calculated pressures are generally even more in disagreement with CsCl pressures (especially > 1100 K), with differences up to 3 GPa at the highest temperatures, even lower than calculated for Mo. Perhaps there are softening processes occurring in the cell assembly that affect the metallic pressure markers at high temperature (and high press load).

The unit cell volume data for the Rb-halide B2-phases are plotted against CsCl pressures in Figures 3 – 5. For a visual inspection, the same volume data are plotted against the Mo-weighted pressures (an average pressure calculated from CsCl and Mo in the three Rb halide samples) in Figures S8 – S10. As shown, the data points increasingly misalign with the BM3-MGD isothermal compression curves (based on CsCl pressures) for temperatures greater than 1100 K. When fitting the BM3-MGD model using Mo-weighted pressures, the model appears to produce large values for the thermal parameter q (~2.5 for RbBr and RbI in Table 1). The parameter q modulates how the Grüneisen parameter (γ) varies with volume, a larger q means that γ changes more rapidly as volume changes and thus the thermal and elastic properties are strongly influenced by compression. Values of q up to ~2 are common for alkali halides due to their relatively soft vibrational modes and significant anharmonic effects under compression[45]. However, values larger than 2 do not appear to be realistic. These large discrepancies suggest that Mo, and particularly Pt, are unreliable pressure markers in LVP cell assemblies at high temperatures (and high press loads). Note, we recognize in Figures 3 – 5, that the calculated CsCl pressures for BT815 at 17-19 GPa exceed the modelled pressures at high temperatures, suggesting the thermal EoS for CsCl might need to be revisited in this HPHT range.

One plausible explanation for the lower apparent pressures reported for Mo and Pt could be related to the strength contrast between the halides and the metals. It is conceivable that crystallites of softer metals, such as Pt, experience lower pressures at high temperatures if CsCl acts as a load-bearing framework. This effect may be less pronounced for Mo, which is stiffer (i.e. possesses a higher Young and shear modulus than Pt) in the halide matrix. Testing this hypothesis with other metals, such as Re or W (hard metals) and Ni (soft metal), in a halide matrix—or avoiding the mixture of these materials altogether—could provide further insights. However, the advantage of mixing metal and halide powders lies in grain boundary pinning, which helps reduce grain growth kinetics and avoid spotty XRD patterns.

Despite these findings, we do not consider the published EoS of Mo [8,31,32] and Pt [28–30] in either DAC or LVP experiments to be particularly problematic, as the results are largely consistent among these studies. Future studies could address the current issue of differential stress in the LVP using AD-XRD with an area detector to collect full radial diffraction patterns, but it is beyond the scope of this study. Finally, we rule out any effect of pressure or temperature gradients, based on similar pressures obtained for Mo in the different samples (Fig. S3) and the close proximity of the thermocouple to the samples.

5.3. Additional Thermodynamic Calculations for RbCl-B2, RbBr-B2, RbI-B2

The BM3-MGD model used in EoSFit7 provides extensive thermodynamic information on the Grüneisen parameter, thermal expansion coefficient, bulk modulus, and heat capacity as functions of pressure and temperature. The B2 phases of RbCl, RbBr, and RbI have not been studied in great detail, although halides were a major focus of research in the 1970s [46]. One prior study using a piston-cylinder apparatus measured RbCl (B1 and B2 phases) and reported the following values at 0.5 GPa for RbCl-B2: γ = 2.13, its derivative q = 2.9, and $(\partial T/\partial P)_S$ = 0.032 K/GPa [47]. While this γ value of

2.13 at 0.5 GPa is nearly consistent with our experimentally determined value of γ = 1.96 at the same pressure, it is lower than the range of values (γ = 2.29–2.88) predicted by various models presented in Ramakrishnan *et al.* [47]. Also, the slope of their γ curve is steeper than that observed in this study (Fig. S11) and their value of *q* is anomalously large, hinting to the limitations of experimental methods more than 40 years ago, and the need to explore larger *P-T* ranges to obtain reliable EoS.

Further calculations using the BM3-MGD model provide additional insights into the thermal expansion coefficient (α), the isothermal and adiabatic bulk moduli (K_T and K_S), and the heat capacities at constant pressure (C_P) and constant volume (C_V). These results, calculated at 1 GPa as a function of temperature, are presented for RbCl-B2, RbBr-B2, and RbI-B2 in Figure S12. To our knowledge, such detailed thermodynamic data for the B2 structures have not been previously published, and are presented here for the first time.

6. Conclusion

We conducted high-pressure, high-temperature experiments to investigate the equations of state (EoS) of rubidium halides (RbCl, RbBr, RbI) in their B2 structures. Using angle-dispersive XRD at beamline P02.2, and energy-dispersive XRD at P61B, we collected diffraction patterns of these halides up to 26 GPa at room temperature in the DAC and up to 21 GPa and 1800 K in the 'Aster-15' LVP, respectively. In the DAC we used ruby fluorescence as a pressure marker, whereas CsCl, Mo and Pt were used in the LVP. The lattice parameters determined for a wide range of P-T conditions allowed us to improve on previous results and to create a very detailed picture of thermal EoS for three halides suggested as reference material for future LVP research.

The third-order Birch-Murnaghan-Mie-Grüneisen-Debye (BM3-MGD) and HT-BM3 EoS were used to model the *P-V-T* data and to explore the effects of different pressure markers on the EoS parameters. The unit cell volume V_0 was constrained by the DAC data at 300 K as V_0 = 36.25(3) cm^3/mol for RbCl, V_0 = 41.74(4) cm^3/mol for RbBr and V_0 = 51.11(2) cm^3/mol for RbI. The optimized EoS and thermoelastic parameters for RbCl, RbBr and RbI are presented in Tables 1 and 2, respectively.

Our results show good agreement between EoS parameters derived from the high-temperature LVP and room-temperature diamond anvil cell (DAC) experiments. However, pressures calculated using Mo and Pt deviate significantly from CsCl pressures at temperatures above 1100 K, suggesting potential discrepancies as a result of their use as pressure markers under these conditions. We further extended our thermodynamic calculations to estimate thermal expansion coefficients, Grüneisen parameters, bulk moduli, and heat capacities for RbCl-B2, RbBr-B2, and RbI-B2 across a wide range of temperatures and pressures. These findings provide new insights into the high-temperature behavior of B2-structured rubidium halides and their potential use as pressure standards for future *in situ* HPHT experiments in the LVP and DAC.

Supplementary Materials

The supplementary text and figures are supplied in a separate document. The information in the document includes a calculation of the Debye temperatures for the B2 rubidium halide phases, 10 additional figures and 7 additional tables. The raw, refined, and model data is located in data files.

Acknowledgements

We acknowledge DESY (Hamburg, Germany), a member of the Helmholtz Association HGF, for the provision of experimental facilities at PETRA-III (LK II, ''G:(DE-HGF)POF4-6G3''). Parts of this research were carried out at beamline P61B (Proposal No. I-20220794). The beamline LVP instrument Aster-15 is funded by the ErUM-Pro programme (grants no.: 05K16WC2 & 05K13WC2) of the German Federal Ministry of Education and Research (BMBF). Parts of the work were conducted at the P02.2. In addition, and we would like to thank R. Njul and A. Röther for assistance in sample preparation for Scanning Electron Microscopy. Mr. Sonntag and Dr. Bhat are thanked for helpful support at the beamline station P61B. This work greatly benefitted from the advice and support of Dr. Boffa Ballaran.

Author Declarations

The authors have no conflicts to disclose.

Data availability

The data that support the findings of this study are available within the article and its supplementary materials.

References

[1] W.A. Bassett, T. Takahashi, and P.W. Stook, "X-Ray Diffraction and Optical Observations on Crystalline Solids up to 300 kbar," Review of Scientific Instruments **38**(1), 37–42 (1967).

[2] D.L. Decker, "High-Pressure Equation of State for NaCl, KCl, and CsCl," Journal of Applied Physics **42**(8), 3239–3244 (1971).

[3] J.M. Brown, "The NaCl pressure standard," Journal of Applied Physics **86**(10), 5801–5808 (1999).

[4] M. Matsui, Y. Higo, Y. Okamoto, T. Irifune, and K.-I. Funakoshi, "Simultaneous sound velocity and density measurements of NaCl at high temperatures and pressures: Application as a primary pressure standard," American Mineralogist **97**(10), 1670–1675 (2012).

[5] Z. Li, and J. Li, "Melting curve of NaCl to 20 GPa from electrical measurements of capacitive current," American Mineralogist **100**(8–9), 1892–1898 (2015).

[6] X. Li, and R. Jeanloz, "Measurement of the *B* 1- *B* 2 transition pressure in NaCl at high temperatures," Phys. Rev. B **36**(1), 474–479 (1987).

[7] Y. Tange, Y. Nishihara, and T. Tsuchiya, "Unified analyses for P-V-T equation of state of MgO: A solution for pressure-scale problems in high P-T experiments," Journal of Geophysical Research: Solid Earth **114**(B3), (2009).

[8] T.S. Sokolova, P.I. Dorogokupets, and K.D. Litasov, "Self-consistent pressure scales based on the equations of state for ruby, diamond, MgO, B2–NaCl, as well as Au, Pt, and other metals to 4 Mbar and 3000 K," Russian Geology and Geophysics **54**(2), 181–199 (2013).

[9] A. Dewaele, A.B. Belonoshko, G. Garbarino, F. Occelli, P. Bouvier, M. Hanfland, and M. Mezouar, "High-pressure--high-temperature equation of state of KCl and KBr," Phys. Rev. B **85**(21), 214105 (2012).

[10] S. Tateno, T. Komabayashi, K. Hirose, N. Hirao, and Y. Ohishi, "Static compression of B2 KCl to 230 GPa and its P-V-T equation of state," American Mineralogist **104**(5), 718–723 (2019).

[11] B.A. Chidester, E.C. Thompson, R.A. Fischer, D.L. Heinz, V.B. Prakapenka, Y. Meng, and A.J. Campbell, "Experimental thermal equation of state of B 2 – KCl," Phys. Rev. B **104**(9), 094107 (2021).

[12] U. Köhler, P.G. Johannsen, and W.B. Holzapfel, "Equation-of-state data for CsCl-type alkali halides," J. Phys.: Condens. Matter **9**(26), 5581–5592 (1997).

[13] C.W.F.T. Pistorius, "Melting Curves of the Rubidium Halides at High Pressures," J. Chem. Phys. **43**(5), 1557–1562 (1965).

[14] P.W. Bridgman, "The pressure transitions of the rubidium halides," in *Papers 59-93*, (Harvard University Press, 1964), pp. 2205–2218.

[15] K.K. Wu, "Pressure induced polymorphic transition in rubidium deuteride," Phys. Stat. Sol. (a) **28**(2), K147–K150 (1975).

[16] A. Dewaele, "Compression of CsCl and CsBr in the megabar range," High Pressure Research **40**(3), 402–410 (2020).

[17] W.A. Crichton, and M. Mezouar, "Noninvasive pressure and temperature estimation in large-volume apparatus by equation-of-state cross-calibration," High Temperatures High Pressures(UK) **34**(2), 235–242 (2002).

[18] R. Farla, "Towards joint *in situ* determination of pressure and temperature in the large volume press exclusively from X-ray diffraction," J Synchrotron Rad **30**(4), 807–814 (2023).

[19] H.-P. Liermann, Z. Konôpková, W. Morgenroth, K. Glazyrin, J. Bednarčik, E.E. McBride, S. Petitgirard, J.T. Delitz, M. Wendt, Y. Bican, A. Ehnes, I. Schwark, A. Rothkirch, M. Tischer, J. Heuer, H. Schulte-Schrepping, T. Kracht, and H. Franz, "The Extreme Conditions Beamline P02.2 and the Extreme Conditions Science Infrastructure at PETRA III," J Synchrotron Rad **22**(4), 908–924 (2015).

[20] R. Farla, S. Bhat, S. Sonntag, A. Chanyshev, S. Ma, T. Ishii, Z. Liu, A. Néri, N. Nishiyama, G.A. Faria, T. Wroblewski, H. Schulte-Schrepping, W. Drube, O. Seeck, and T. Katsura, "Extreme conditions research using the large-volume press at the P61B endstation, PETRA III," J Synchrotron Rad **29**(2), 409–423 (2022).

[21] D.R. Black, M.H. Mendenhall, C.M. Brown, A. Henins, J. Filliben, and J.P. Cline, "Certification of Standard Reference Material 660c for powder diffraction," Powder Diffr. **35**(1), 17–22 (2020).

[22] R. Boehler, and K. De Hantsetters, "New anvil designs in diamond-cells," High Pressure Research **24**(3), 391–396 (2004).

[23] G. Shen, Y. Wang, A. Dewaele, C. Wu, D.E. Fratanduono, J. Eggert, S. Klotz, K.F. Dziubek, P. Loubeyre, O.V. Fat'yanov, P.D. Asimow, T. Mashimo, and R.M.M. Wentzcovitch, "Toward an international practical pressure scale: A proposal for an IPPS ruby gauge (IPPS-Ruby2020)," High Pressure Research **40**(3), 299–314 (2020).

[24] J. Hernlund, "A numerical model for steady-state temperature distributions in solid-medium high-pressure cell assemblies," American Mineralogist **91**(2–3), 295–305 (2006).

[25] Y. Nishihara, S. Doi, S. Kakizawa, Y. Higo, and Y. Tange, "Effect of pressure on temperature measurements using WRe thermocouple and its geophysical impact," Physics of the Earth and Planetary Interiors **298**, 106348 (2020).

[26] B.H. Toby, and R.B. Von Dreele, "*GSAS-II* : the genesis of a modern open-source all purpose crystallography software package," J Appl Crystallogr **46**(2), 544–549 (2013).

[27] R. Myhill, S. Cottaar, T. Heister, I. Rose, C. Unterborn, J. Dannberg, and R. Gassmoeller, "BurnMan – a Python toolkit for planetary geophysics,geochemistry and thermodynamics," JOSS **8**(87), 5389 (2023).

[28] Y. Fei, A. Ricolleau, M. Frank, K. Mibe, G. Shen, and V. Prakapenka, "Toward an internally consistent pressure scale," Proceedings of the National Academy of Sciences **104**(22), 9182–9186 (2007).

[29] C.-S. Zha, K. Mibe, W.A. Bassett, O. Tschauner, H.-K. Mao, and R.J. Hemley, "P - V - T equation of state of platinum to 80GPa and 1900K from internal resistive heating/x-ray diffraction measurements," Journal of Applied Physics **103**(5), 054908 (2008).

[30] M. Matsui, E. Ito, T. Katsura, D. Yamazaki, T. Yoshino, A. Yokoyama, and K. Funakoshi, "The temperature-pressure-volume equation of state of platinum," Journal of Applied Physics **105**(1), 013505 (2009).

[31] K.D. Litasov, P.I. Dorogokupets, E. Ohtani, Y. Fei, A. Shatskiy, I.S. Sharygin, P.N. Gavryushkin, S.V. Rashchenko, Y.V. Seryotkin, Y. Higo, K. Funakoshi, A.D. Chanyshev, and S.S. Lobanov, "Thermal equation of state and thermodynamic properties of molybdenum at high pressures," Journal of Applied Physics **113**(9), 093507 (2013).

[32] X. Huang, F. Li, Q. Zhou, Y. Meng, K.D. Litasov, X. Wang, B. Liu, and T. Cui, "Thermal equation of state of Molybdenum determined from in situ synchrotron X-ray diffraction with laser-heated diamond anvil cells," Sci Rep **6**(1), 19923 (2016).

[33] J. Gonzalez-Platas, M. Alvaro, F. Nestola, and R. Angel, "*EosFit7-GUI* : a new graphical user interface for equation of state calculations, analyses and teaching," J Appl Crystallogr **49**(4), 1377–1382 (2016).

[34] R.J. Angel, M. Alvaro, and F. Nestola, "40 years of mineral elasticity: a critical review and a new parameterisation of equations of state for mantle olivines and diamond inclusions," Phys Chem Minerals **45**(2), 95–113 (2018).

[35] F. Birch, "Elasticity and constitution of the Earth's interior," J. Geophys. Res. **57**(2), 227–286 (1952).

[36] P. Vinet, J. Ferrante, J.H. Rose, and J.R. Smith, "Compressibility of solids," J. Geophys. Res. **92**(B9), 9319–9325 (1987).

[37] Y. Fei, "Thermal Expansion," in *AGU Reference Shelf*, edited by T.J. Ahrens, (American Geophysical Union, Washington, D. C., 1995), pp. 29–44.

[38] V.N. Zharkov, and V.A. Kalinin, *Equations of State for Solids at High Pressures and Temperatures* (Springer US, Boston, MA, 1971).

[39] O.L. Anderson, *Equations of State of Solids for Geophysics and Ceramic Science* (Oxford University Press, 1995).

[40] F.D. Stacey, and P.M. Davis, "High pressure equations of state with applications to the lower mantle and core," Physics of the Earth and Planetary Interiors **142**(3–4), 137–184 (2004).

[41] T. Kumara Swamy, K. Srinivas, K.G. Subhadra, and D.B. Sirdeshmukh, "Debye–Waller factors and Debye temperatures of rubidium halides," Acta Crystallogr A Found Crystallogr **52**(1), 88–90 (1996).

[42] O.L. Anderson, "A simplified method for calculating the debye temperature from elastic constants," Journal of Physics and Chemistry of Solids **24**(7), 909–917 (1963).

[43] C. Prescher, and V.B. Prakapenka, "*DIOPTAS* : a program for reduction of two-dimensional X-ray diffraction data and data exploration," High Pressure Research **35**(3), 223–230 (2015).

[44] V. Petříček, M. Dušek, and L. Palatinus, "Crystallographic Computing System JANA2006: General features," Zeitschrift Für Kristallographie - Crystalline Materials **229**(5), 345–352 (2014).

[45] T. Sumita, and A. Yoneda, "Anharmonic effect on the equation of state (EoS) for NaCl," Phys Chem Minerals **41**(2), 91–103 (2014).

[46] S.N. Vaidya, and G.C. Kennedy, "Compressibility of 27 halides to 45 kbar," Journal of Physics and Chemistry of Solids **32**(5), 951–964 (1971).

[47] J. Ramakrishnan, R.J. Hardy, and G.C. Kennedy, "The Grüneisen parameter γ of KBr, RbCl and Bi through high pressure phase transitions," Journal of Physics and Chemistry of Solids **40**(4), 297–303 (1979).